ELSEVIER

Journal of Photochemistry and Photobiology A: Chemistry 135 (2000) 185–191

Journal of Photochemistry and Photobiology A:Chemistry

www.elsevier.nl/locate/jphotochem

Photophysical and photoelectrochemical properties of the bis(2,2′-bipyridine)(4,4′-dimethylthio-2,2′-bipyridine)ruthenium(II) complex

Henrique E. Toma [a,*], Ricardo M. Serrasqueiro [a], Reginaldo C. Rocha [a], Gregoire J.F. Demets [a], Herbert Winnischofer [a], Koiti Araki [a], Paulo E.A. Ribeiro [b], Claudio L. Donnici [b]

[a] *Instituto de Química, Universidade de São Paulo, Caixa Postal 26077 CEP 05513-970, São Paulo, SP, Brazil*
[b] *Departamento de Química, ICEX, Universidade Federal de Minas Gerais, Belo Horizonte, MG, Brazil*

Received 13 April 2000; accepted 19 April 2000

Abstract

The chemistry and photophysics of a new ruthenium(II)–polypyridine complex, $[Ru(bipy)_2(Sbipy)]^{2+}$ where bipy=2,2′-bipyridine and Sbipy=4,4′-dimethylthio-2,2′-bipyridine, have been investigated. In spite of the thioether substituents in the 4,4′ positions of the 2,2′-bipyridine ligand, this complex behaves similarly to the $[Ru(bipy)_3]^{2+}$ complex, exhibiting strong charge-transfer bands at 450 nm, and luminescence emission at 630 nm ($t_{1/2}$=0.91 μs), at room temperature. The time resolved excited state spectrum was simulated using the open-shell ZINDO/S method, indicating a rather complex composition of metal-to-ligand, ligand-to-metal and ligand-to-ligand charge-transfer transitions. The thioether groups have been exploited as strong binding sites for pentacyanoferrate ions, allowing the generation of polynuclear species suitable for immobilization purposes, onto nickel electrode surfaces. Such Prussian blue type films displayed photoaction response to visible light in the presence of dissolved oxygen.

Keywords: Ruthenium polypyridines; Polynuclear complexes; Pentacyanoferrate; Electrochemistry; Photoelectrochemistry

1. Introduction

Ruthenium(II) polypyridine complexes have been extensively investigated in the last two decades because of their remarkable chemical, and photophysical properties [1–3]. In particular, complexes containing bipyridine ligands with carboxylate substituents at 4,4′-positions have received special attention due to their great facility to adsorb onto nanocrystalline TiO_2 particles, thus providing suitable photoanodes for high performance solar cells [4–6]. Ferrere and Gregg [7] have shown that the sensitization process can be extremely fast, from the efficient photoaction response observed in the case of the ultra-short lived, non-emissive excited state of the *cis*-$[Fe^{II}$(2,2′-bipyridine-4,4′-dicarboxylate$)_2(CN)_2]$ complex. Consequently, there is an intrinsic interest on polypyridine complexes bearing substituents which can directly bind onto the TiO_2 and other wide band-gap oxide semiconductor surfaces, improving the energy transfer mechanism or/and widening the useful solar spectral range. Immobilization of ruthenium(II) polypyridine complexes onto Prussian blue type films [8,9] can also provide an interesting, alternative way of obtaining photoelectrochemically active materials, as previously reported in the literature [10].

In this work, we focused on the chemistry and photophysics of a new ruthenium(II)–polypyridine complex containing thiomethyl groups at the 4,4′-positions of the bipyridine ring (Fig. 1). To our knowledge ruthenium(II)–polypyridine complexes exhibiting sulfur containing substituents have never been reported in the literature. In special, thioether groups are known to be rather effective binding sites for pentacyanoferrate(II) [11] and many platinum group metals complexes. By attaching pentacyanoferrate(II) complexes to the peripheral binding sites of the ruthenium(II)–polypyridine complex, the immobilization of the photoactive species as Prussian blue type films has been pursued with great interest, in view of their expected photoelectrochemical behavior.

2. Experimental section

2.1. Synthesis

4,4′-dimethylthio-2,2′-bipyridine (Sbipy) was synthesized by reacting 1.00 g (3.95 mmol) of 4,4′-dichloro-2,2′-bipyri-

* Corresponding author.

1010-6030/00/$ – see front matter
PII: S1010-6030(00)00293-8

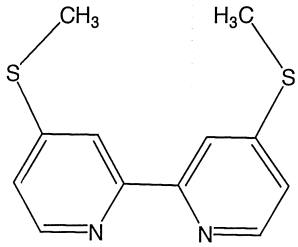

Fig. 1. The 4,4′-dimethylthio-2-2′-bipyridine ligand.

dine with a sodium methanethiolate solution containing 2.6 g of NaH (60% in mineral oil), 60 cm^3 of anhydrous methanol and 3.70 cm^3 of methanethiol, in a flask equipped with magnetic stirring and reflux condenser. The mixture was heated at reflux for 30 h. After filtration and recrystallization from ethanol, 0.63 g (69%) of the light yellow product was obtained. m.p. 153–155°C; ^{1}H NMR (d, $CDCl_3$): 8.47 (2H, d, $H_6H_{6'}$ J=5.4 Hz), 8.27 (2H, d, $H_3H_{3'}$ J=1.9 Hz), 7.15 (2H, dd, J=5.4 and 1.9 Hz, $H_5H_{5'}$) and 2.60 (2H, s, SMe); ^{13}C NMR (d, $CDCl_3$): 155.34 (C_2), 151.41 (C_4), 148.33 (C_3), 120.08 (C_6), 117.12 (C_5), 13.82 (SMe). Analytically calculated for $C_{12}H_{12}N_2S_2$: C, 58.05; H, 4.85; N, 11.33. Found: C, 58.24; H, 4.87; N, 11.40.

[Ru(bipy)$_2$(Sbipy)](PF$_6$)$_2$ complex was synthesized by refluxing 5 cm^3 of a (2:3 v/v) water/ethanol solution containing 30 mg (0.060 mmol) of $Ru(bipy)_2Cl_2{\cdot}2H_2O$ and 17 mg (0.068) mmol of Sbipy, for 2 h, under an argon atmosphere. The solution was concentrated to 2 cm^3 in a flash-evaporator, and precipitated as an orange-red solid after addition of 200 mg of NH_4PF_6. The product was collected on a filter, washed with small amounts of cold water and diethyl ether, and dried under vacuum. Analytically calculated for $RuC_{32}H_{28}N_6S_2P_2F_{12}$: C, 40.3; H, 3.0; N, 8.8. Found: C, 39.2; H, 3.0; N, 8.6.

2.2. Physical measurements

The electronic spectra of the complexes were recorded on a Hewlett–Packard model 8453-A diode-array spectrophotometer, or on a Guide-Wave model 260 fiber-optics instrument. Cyclic voltammetry measurements were carried out with a Princeton Applied Research model 283 potentiostat, using a conventional three electrode cell arrangement [8]. A platinum electrode working electrode was employed along with a Luggin capillary with $Ag/AgNO_3$ (0.010 mol dm^{-3}) reference electrode (E^0=0.503 versus SHE) [12] and a coiled platinum wire auxiliary electrode, both in DMF or acetonitrile solutions, containing 0.10 mol dm^{-3} Et_4NClO_4.

Emission and excitation spectra were recorded on a Photon Technology model LS100 spectrofluorometer. Lifetime and excited state differential spectra were obtained using a flash-photolysis equipment from Edinburgh Analytical Instruments model LP900S1. It consisted of a pulsed Surelite II-10 laser (width ≅5 ns), and an optical analyser based on a 500 W xenon lamp, a Czern–Turner monochromator (250–900 nm range), and a Hamamatsu R955 photomultiplier. Transient signals were captured on a Tektronix TDS 520 digital oscilloscope, interfaced to an IBM/PC computer through an IEEE-488 interface. The excited state spectrum was obtained from the differential spectrum by summing the ground state spectrum in such a way to make the absorbance of the excited state species coincident with of the ground state one at the points where the differential spectrum were equal to zero.

The Prussian Blue type films were grown onto a nickel electrode surface by cycling the potentials in the −0.2 to 1.0 V range for 30 min, at 50 mV s^{-1}, in a 0.5 mmol dm^{-3} solution of $[(CN)_5Fe(\mu\text{-Sbipy})Ru(bipy)_2]^-$. The binuclear complex was prepared in situ by mixing equimolar amounts of the $Na_3[Fe(CN)_5(NH_3)]{\cdot}3H_2O$ and $[Ru(bipy)_2(Sbipy)](PF_6)_2$ complexes, in aqueous solution containing 0.5 mol dm^{-3} KNO_3. Exploratory photocurrent measurements were carried out using a PAR model 366 bipotentiostat connected to a HP7090A plotter, by applying a bias potential of −0.50 V while the films were directly irradiated with an overhead projector light source.

2.3. Molecular calculations

Semiempirical theoretical calculations were carried out with the ZINDO/97 program [13] from MSI [14]. SCF molecular orbitals were obtained, at the RHF and ROHF levels for the closed-shell (ground state) and open-shell (excited state) species, by using the INDO/S Hamiltonian [15] (ZINDO/S method). Atomic parameterization for ruthenium was employed as described elsewhere [16]. The default values $f_{\sigma-\sigma}$=1.267 and $f_{\pi-\pi}$=0.585 were used to account for the interactions. Electronic spectra were generated by CI (from the singlet ground state) or Rumer-CI [17] (from the lowest triplet excited state) calculations employing 200 singly excited configuration state functions generated from the top 10 occupied MO into the lowest 10 empty MO levels, plus the SCF ground state. The molecular structures used in the quantum calculations were initially obtained from the geometry optimizations at molecular mechanics level by using the MM+ module [18] within the HyperChem 5.1 program [19]. Further refinement was carried out by ZINDO/1 semiempirical method at RHF or UHF level, for the ground and excited states, respectively. A gradient of 1.0 cal $Å^{-1}$ mol^{-1} was used as a convergence criterion in a conjugate gradient algorithm. The obtained results showed an excellent agreement with the experimental data [16] for similar complexes (Ru–N distances, for instance, lie in the range from 2.0 to 2.1 Å). The calculations were processed either on a SGI Indigo^2 R10000 workstation (IRIX/ZINDO) or on a Pentium III PC (Windows/HyperChem).

All the theoretical results presented below refer to calculations in vacuum. Calculations considering solvation by dimethylformamide and acetonitrile were also performed through the SCRF method [20]. Nevertheless, no significant

changes in the spectrum were observed and will not be reported.

3. Results and discussion

3.1. Mononuclear species

The $[Ru(bipy)_2(Sbipy)]^{2+}$ complex exhibits a characteristic composite absorption band at 450 nm, followed by inflections at 370 and 325 nm, and a strong band at 280 nm, as illustrated in Fig. 2a. Because of the presence of mixed bipyridine ligands, a detailed theoretical analysis was carried out for this complex, using INDO-based semiempirical methods, as described in Section 2. The ZINDO/1 optimized structure of $[Ru(bipy)_2(Sbipy)]^{2+}$ in the ground state is illustrated in Fig. 3. The ZINDO/S simulation results and assignment of the electronic transitions can be seen in Tables 1 and 2, where the composition of the several electronic levels involved has been specified.

According to the theoretical calculations, the main band at 430 (sh) and 455 nm is dominated by the ruthenium-to-bipy and ruthenium-to-Sbipy charge-transfer transitions from the three predominantly metal d_π orbitals (MO 100–102) to the combined π^* levels (also referred as π_1^* levels) of the bipy and Sbipy ligands (MO 103–105). The inflections in the near UV region involved another set of ruthenium-to-bipy

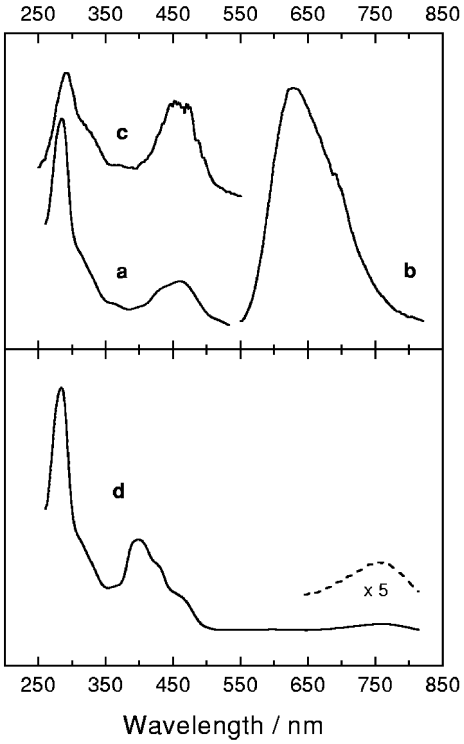

Fig. 2. Ground state (a) absorption, (b) emission and (c) excitation spectra; and (d) excited state absorption spectrum of the $[Ru(bipy)_2(Sbipy)]^{2+}$ complex in acetonitrile.

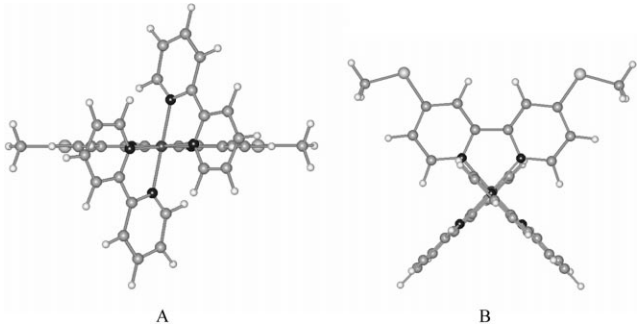

Fig. 3. Ground state molecular structure of the $[Ru(bipy)_2(Sbipy)]^{2+}$ complex (A) side view, (B) top view.

(and Sbipy) charge-transfer transitions, from the predominantly metal d_π orbitals to π^* levels of higher energy (also referred as π_2^* levels) in the bipy and Sbipy ligands (MO 106 and 107). The strong band in the UV region is ascribed to $\pi \rightarrow \pi^*$ transitions internal of the bipy and Sbipy ligands. An important conclusion from Table 1, is that the bipy and Sbipy levels are strongly mixed in the complex. Therefore, the electronic excitation in the charge-transfer bands should lead to the population of the electronic levels localized in both ligands, as in the symmetric $[Ru(bipy)_3]^{2+}$ complex.

The luminescence spectrum of the $[Ru(bipy)_2(Sbipy)]^{2+}$ complex (Fig. 2b) exhibits a strong band at 630 nm, which can be ascribed to the emission from the lowest triplet excited state, by analogy with $[Ru(bipy)_3]^{2+}$ complex. The corresponding excitation profile (Fig. 2c) is very similar to the absorption spectrum (Fig. 2a), indicating efficient internal conversion and intersystem crossing processes involving the several excited states in the complex. Lifetime measurements carried out in DMF solutions were consistent with a single exponential emission decay ($t_{1/2}$=0.91 μs), accompanied by the recovery of the starting absorption spectra after the bleaching induced by the laser pulse. The emission quantum yield of 0.021 was determined using the known quantum yield of the $[Ru(bipy)_3]^{2+}$ complex (Φ_{em}=0.068) [1] and the relative integrated areas corrected by the relative absorbances at the excitation wavelength. Both, luminescence intensity and lifetime values were strongly dependent on the presence of dissolved dioxygen in solution, as shown in Fig. 4. Singlet oxygen emissions have been detected in such experiments ($t_{1/2}$=76.1 μs), using a previously reported experimental arrangement [21]. This results strongly suggests that there is an efficient energy transfer process from the complex triplet excited state to the dioxygen molecule (Fig. 4 — inset).

The excited state absorption spectrum has also been obtained from the flash-photolysis measurements, as illustrated in Fig. 2d. The assignment of the excited state spectrum has been carried out based on the ZINDO/S theoretical calculations (see Section 2) and summarized in Table 2. The semi-occupied frontier orbitals, MO number 102 (SOMO — singly occupied molecular orbital) and 103 (SHOMO —

Table 1
Energy, symmetry and composition of the singlet ground state molecular orbitals of the $[Ru(bpy)_2(Sbipy)]^{2+}$ complex

MO index	Energy (eV)	Symmetry	Ru (%)	$bipy_1$ (%)	$bipy_2$ (%)	Sbipy (%)
107	−5.537	*a*	1.70	45.87	45.88	6.54
106	−5.560	*b*	0.73	48.97	48.95	1.35
105	−6.222	*b*	6.44	10.14	10.14	73.27
104	−6.265	*a*	7.44	45.91	45.90	0.75
LUMO	−6.486	*b*	0.26	38.92	38.91	21.91
HOMO	−12.446	*b*	59.03[a]	8.75	8.75	23.46
101	−12.505	*a*	60.98[b]	14.72	14.71	9.59
100	−12.594	*a*	66.66[c]	11.70	11.70	9.94
99	−13.800	*b*	0.27	49.14	49.16	1.43
98	−13.806	*a*	0.39	12.96	12.94	73.71

[a] $0.41607d_{z^2} - 0.31818d_{xz} + 0.40614d_{yz} + 0.38748\ d_{x^2-y^2} - 0.02097d_{xy}$.
[b] $-0.10388d_{z^2} + 0.42493d_{xz} + 0.47144d_{yz} - 0.00974d_{x^2-y^2} + 0.44217d_{xy}$.
[c] $-0.42732d_{z^2} + 0.20984d_{xz} + 0.05473d_{yz} + 0.55450d_{x^2-y^2} - 0.35661d_{xy}$.

singly highest occupied molecular orbital), exhibit predominant Ru d_π and bipy (π) character, respectively, as expected for a MLCT excited state. However, our calculation results showed that the weak band around 750 nm corresponds to an electronic transition from the semi-occupied MO 102 to the excited level MO 113, both exhibiting large Ru d_π character instead of the conventionally assigned transition from $bipy^-$ to bipy π^* levels. Furthermore, the series of absorption bands in the 400–460 nm region involve a rather complex mixture of electronic transitions from the occupied, predominantly metal d_π levels (MO 100–102), bipy (MO 98 and 99) and Sbipy (MO 97) levels, to the empty bipy (MO 104) and Sbipy (MO 105) π^* levels. Nevertheless, substantial contributions from the semi-occupied levels (MO 102 and 103) were also found. The sharp absorption band around 285 nm involved $\pi \rightarrow \pi^*$ electronic transitions from the predominantly bipy π (MO 98) to the empty bipy π^* (MO 104) orbital, with significant participation of the semi-occupied

Table 2
Experimental and theoretical spectra of $[Ru(bpy)_2(Sbipy)]^{2+}$ in the ground state

Experimental		Calculated		Transition[a] $MO_i \rightarrow MO_f$
λ (nm)	ε ($M^{-1}\,cm^{-1}$)	λ (nm)	Osc. strength	
455	1.6×10^4	455	0.168	#101→#103 (*B*)
		454	0.090	#101→#105 (*B*)
				#100→#105 (*B*)
		450	0.157	#102→#103 (*A*)
				#100→#104 (*A*)
430	1.3×10^4	441	0.198	#102→#105 (*A*)
				#101→#104 (*A*)
395	6.8×10^3	–	–	–
370	7.9×10^3	377	0.083	#102→#105 (*A*)
				#101→#104 (*A*)
				#100→#107 (*A*)
325	1.7×10^4	332	0.205	#102→#107 (*B*)
				#100→#106 (*B*)
		330	0.205	#102→#107 (*B*)
				#101→#106 (*B*)
305	2.5×10^4	295	0.310	#98→#103 (*B*)
				#98→#105 (*B*)
		290	0.329	#99→#103 (*A*)
280	6.9×10^4	272	1.500	#99→#104 (*B*)
				#98→#105 (*B*)

[a] The transition symmetry is given in parentheses.

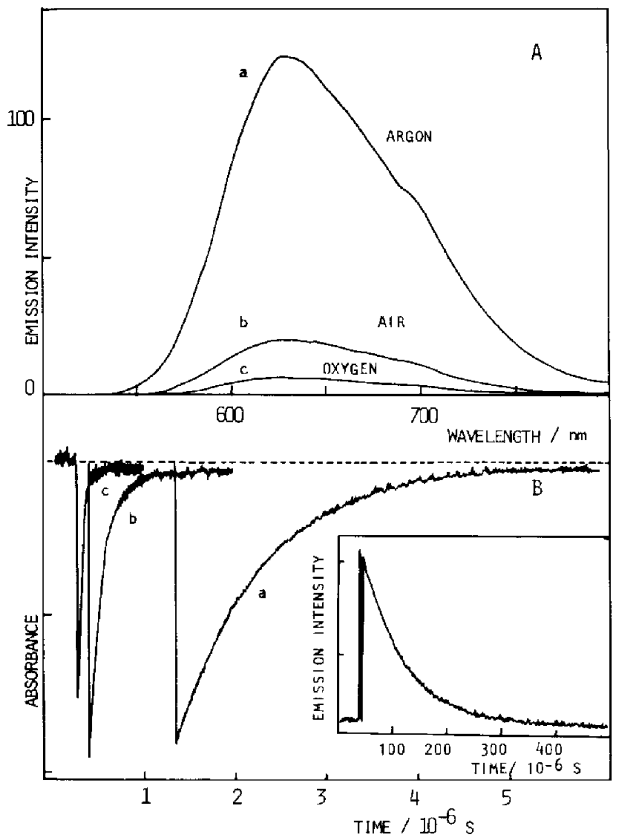

Fig. 4. Emission spectra (A), and excited state decay curves (B) of the $[Ru(bipy)_2(Sbipy)]^{2+}$ complex (0.01 $mmol^{-3}$) in (a) argon, (b) air and (c) oxygen saturated DMF solutions: Inset: singlet oxygen emission measured at 1270 nm.

bipy$^-$ (MO 103) and Ru d_π (MO 102) levels. As shown in the above discussion, in contrast with the ground state absorption spectrum in which the transitions involved more or less localized ground and excited states, the transitions from the triplet excited state involve electronic states constituted by a rather complex mixture of the ligands and metal orbitals. This is a consequence of the pronounced Ru^{III} and bipy$^-$ character of the species generated after the laser pulse, i.e. $[Ru^{III}(bipy^-)(bipy)(Sbipy)]^{2+*}$, and probably of its ambiguous oxidizing/reducing character (Tables 3 and 4).

The cyclic voltammograms of the $[Ru(bipy)_2(Sbipy)]^{2+}$ complex are shown in Fig. 5. In organic solvents such as dimethylformamide and acetonitrile, the oxidation of the ruthenium(II) center proceeds reversibly at 1.30 V; while the monoelectronic reduction of each of the three ligands occurs at −1.17, −1.33 and −1.62 V. At higher positive potentials, near the limit of working conditions, a chemically irreversible process can be detected from an anodic peak at 2.3 V. This process leads to the decay of the $Ru^{III/II}$ wave at 1.30 V, with the rise of another reversible wave at 1.45 V, which can be ascribed to the electrochemical oxidation of the thiomethylbipyridine ligand to the corresponding sulfoxide derivative.

From the emission spectrum and electrochemical results, one can estimate the redox potentials of the excited species, [22] based on the equations:

$$E^0\left(\frac{D^+}{D^*}\right) = E^0\left(\frac{D^+}{D}\right) - E_{00}$$

$$E^0\left(\frac{D^*}{D^-}\right) = E^0\left(\frac{D}{D^-}\right) + E_{00}$$

where D refers to the $[Ru(bipy)_2(Sbipy)]^{2+}$ complex and E_{00} represents the excited state energy, in eV. The calculated values of $E^0(D^+/D^*)$ and $E^0(D^*/D^-)$ were −0.67 and 0.80 V, respectively, in DMF or acetonitrile solutions, indicating that the excited complex is a relatively strong reducing and oxidizing species.

3.2. Polynuclear species and films

As expected from the presence of the thioether groups, the $[Ru(bipy)_2(Sbipy)]^{2+}$ complex strongly bind pentacyanoferrate(II) ions at the sulphur atom, as illustrated in Fig. 6. This reaction can be readily followed by cyclic voltammetry, because of the appearance of a new reversible wave at 0.6 V, attributed to the Fe(III/II) pair. The great stability of pentacyanoferrate(II) complexes with ligands containing thioether groups, such as methionine, has already been reported in the literature [23].

The formation of the pentacyanoferrate(II)-$[Ru(bipy)_2(Sbipy)]^{2+}$ film onto a nickel electrode by cycling the potentials in the −200 to 1000 mV range, can be monitored by the rise of a broad wave at 0.65 V as a function of the number of cycles. During this procedure, Ni^{2+} ions are released from the electrode surface, leading to the immobilization of the $[(CN)_5Fe(\mu\text{-}Sbipy)Ru(bipy)_2]^-$ complex through the formation of Prussian Blue type materials containing Ni–NC–Fe bonds [8,9]. After cycling the potentials for 30 min at 50 mV s^{-1}, the modified electrodes were removed from the solution and washed with water. The electronic spectrum of the adsorbed film exhibited the characteristic MLCT band of the immobilized $[Ru(bipy)_2(Sbipy)]^{2+}$ complex, around 450 nm.

The incorporation of the photoactive tris-bipyridine ruthenium(II) complex into the nickel Prussian blue films turned them photoelectrochemically active, as reflected in the observed photoaction response in the presence of dioxygen.

Table 3
Energy, symmetry and composition of the lowest triplet excited state molecular orbitals of the $[Ru(bpy)_2(Sbipy)]^{2+}$ complex

MO index	Energy (eV)	Symmetry	Ru (%)	$bipy_1$ (%)	$bipy_2$ (%)	Sbipy (%)
114	−4.362	*a*	49.96[a]	21.07	21.07	7.91
113	−4.431	*b*	48.94[b]	11.35	11.35	28.36
107	−5.617	*a*	0.67	47.31	47.31	4.70
106	−5.739	*a*	0.81	2.41	2.41	94.37
105	−6.609	*b*	2.61	0.47	0.47	96.45
104	−7.033	*a*	3.76	47.94	47.94	0.36
SHOMO	−9.933	*b*	1.04	49.09	49.09	0.79
SOMO	−15.278	*a*	82.12[c]	6.16	6.16	5.55
101	−13.522	*b*	34.15[d]	22.59	22.59	20.67
100	−13.600	*a*	44.24[e]	22.67	22.67	10.43
99	−13.848	*b*	12.17[f]	36.46	36.46	14.90
98	−13.922	*a*	6.01	46.22	46.22	1.56
97	−14.364	*a*	0.22	1.12	1.12	97.53

[a] $0.39440d_{z^2}+0.56579\ d_{x^2-y^2}+0.15433d_{xy}$.
[b] $0.69837d_{xz}+0.01438d_{yz}$.
[c] $0.42328d_{z^2}-0.07816\ d_{x^2-y^2}-0.79515d_{xy}$.
[d] $0.58316d_{yz}-0.03372d_{xy}$.
[e] $-0.46170d_{z^2}+0.36962\ d_{x^2-y^2}-0.30373d_{xy}$.
[f] $-0.01845d_{xz}+0.34832d_{yz}$.

Table 4
Experimental and theoretical spectra of $[Ru(bpy)_2(Sbpy)]^{2+}$ in the lowest excited triplet state

Experimental		Calculated		Transition[a,b]
λ (nm)	ε ($M^{-1}\,cm^{-1}$)	λ (nm)	Osc. Strength	$MO_i \rightarrow MO_f$
750	6.0×10^3	670	0.002	#102→#113 (*B*)
460	3.3×10^4	469	0.022	#99→#103 (*A*) #101→#103 (*A*)
		460	0.034	#98→#103 (*B*) #98→#107 (*B*)
425	6.6×10^4	423	0.014	#100→#104 (*B*) #100→#102 (*B*)
		421	0.010	#101→#104 (*A*) #101→#102 (*A*)
400	8.8×10^4	384	0.064	#103→#104 (*A*) #101→#104 (*A*) #99→#104 (*A*)
		374	0.045	#101→#105 (*B*) #101→#102 (*B*) #98→#104 (*B*)
		366	0.017	#99→#104 (*A*) #100→#102 (*A*) #98→#102 (*A*)
		365	0.025	#97→#103 (*B*) #101→#105 (*B*) #101→#102 (*B*)
330	6.7×10^4	335	0.011	#99→#103 (*A*) #103→#104 (*A*)
315	8.5×10^4	326	0.140	#103→#105 (*B*) #101→#105 (*B*) #101→#102 (*B*)
285	2.4×10^5	307	0.026	#101→#102 (*B*) #99→#102 (*B*) #103→#104 (*B*)
		305	0.181	#98→#104 (*B*) #103→#104 (*B*) #98→#102 (*B*)

[a] The transition symmetry is given in parentheses.
[b] Only the first three most important components for each transition are shown.

Typical results during a sequential exposition to visible light and dark, at a bias potential of −0.5 V, in oxygen or air saturated aqueous solutions, are shown in Fig. 7.

The rise time and limiting current of the photocurrent after the beginning of the irradiation step was found to be rather reproducible. In spite of the slow photoresponse, the limiting currents were proportional to the concentration of dissolved oxygen and to the light intensity. Furthermore, the photocurrent did not drop abruptly to zero when the irradiation was interrupted, but rather decreased exponentially to zero. This residual photocurrent in the dark probably arises from trapped charges remaining after the photoexcitation process. A possible mechanism consistent with these facts is presented below (Eqs. (1)–(4)):

$$[Ni_x\text{-}(CN)_5Fe^{II}(\mu\text{-}Sbipy)Ru^{II}(bipy)_2)] + h\nu \rightarrow [Ni_x\text{-}(CN)_5Fe^{II}(\mu\text{-}Sbipy)Ru^{III}(bipy^-)_2]^* \quad (1)$$

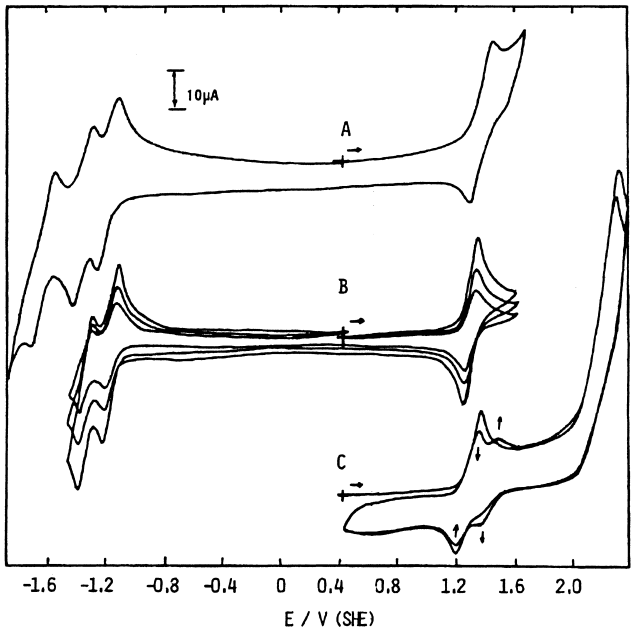

Fig. 5. Cyclic voltammograms of the $[Ru(bipy)_2(Sbipy)]^{2+}$ complex (5 mmol dm^{-3}) in (A) DMF, at 50 mV s^{-1}, showing the $Ru^{III/II}$ redox waves at $E_{1/2}$=1.30 V, and the bipy and Sbipy reduction waves at −1.17, −1.33 and −1.62 V (B) acetonitrile solution, at scan rates 10, 20 and 50 mV s^{-1}, (C) acetonitrile solution, at 50 mV s^{-1}, showing the oxidation wave at 1.3 V and formation of the sulfoxide derivative at $E_{1/2}$=1.45 V.

$$[Ni_x\text{-}(CN)_5Fe^{II}(\mu\text{-}Sbipy)Ru^{III}(bipy^-)_2]^* + \tfrac{1}{2}O_2 + H^+ \rightarrow [Ni_x\text{-}(CN)_5Fe^{II}(\mu\text{-}Sbipy)Ru^{III}(bipy)_2] \quad (2)$$

$$[Ni_x\text{-}(CN)_5Fe^{II}(\mu\text{-}Sbipy)Ru^{III}(bipy)_2] \rightarrow [Ni_x\text{-}(CN)_5Fe^{III}(\mu\text{-}Sbipy)Ru^{II}(bipy)_2] \quad (3)$$

$$[Ni_x\text{-}(CN)_5Fe^{III}(\mu\text{-}Sbipy)Ru^{II}(bipy)_2] + e^- \rightarrow [Ni_x\text{-}(CN)_5Fe^{II}(\mu\text{-}Sbipy)Ru^{II}(bipy)_2] \quad (4)$$

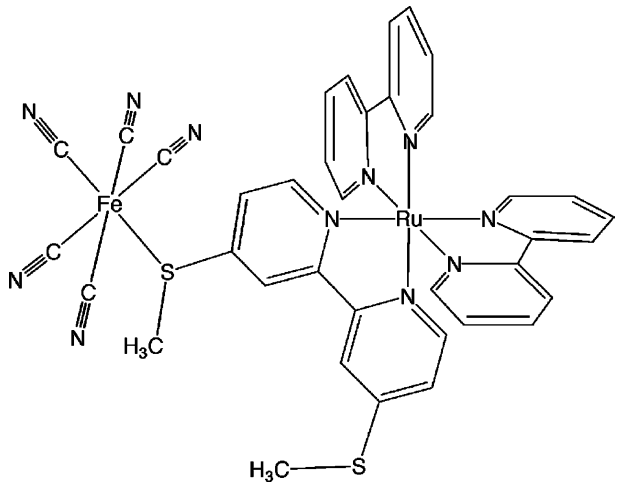

Fig. 6. Structural representation of the $[(CN)_5Fe(\mu\text{-}Sbipy)Ru(bipy)_2]^-$ species.

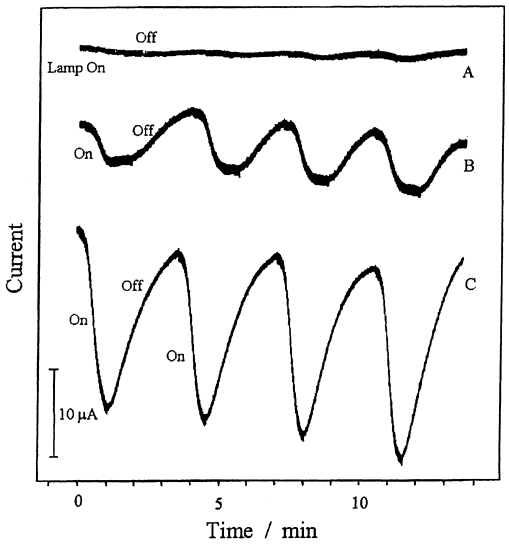

Fig. 7. Successive photochronoamperometric curves at $E=-0.55$ V, for the nickel-[$(CN)_5Fe(\mu$-Sbipy)$Ru(bipy)_2$] film under white lamp illumination (on), and in the dark (off) recorded in (A) argon, (B) air and (C) oxygen saturated water, 0.5 mol dm^{-3} KNO_3, bare starting nickel electrode area=0.30 cm^2.

By analogy with the $[Ru(bipy)_2(Sbipy)]^{2+}$ complex, the excited species formed in step (1) should be a strong reducing agent, reacting rapidly with dioxygen in order to generate the charge-separated $[Ni_x$-$(CN)_5Fe^{II}(\mu$-Sbipy$)Ru^{III}(bipy)_2]$ species (step 2). Intramolecular electron transfer (step 3) is thermodynamically favored, from the expected difference of 0.7 V in the redox potentials of the iron(II) and ruthenium(III) centers. This process is important for the observation of the current flow (step 4) from the electrode. However, steps (3) and (4) seem to be relatively slow, as deduced from the observed slow increase and decrease of the photocurrents after the irradiation and dark onset, respectively, as shown in Fig. 5. Further studies will be necessary to elucidate this point.

In conclusion, the strategy of employing thioether substituents as strong binding sites for cyanoferrate ions was successful, allowing the immobilization of ruthenium(II)–polypyridine complexes into nickel Prussian blue films. The pronounced photocurrent response to visible light in the presence of dissolved oxygen was particularly remarkable when compared with previously reported tris-bipyrazine ruthenium(II) analogue [10,24], suggesting possible applications in photoelectrochemical sensors and devices.

Acknowledgements

The support from John Simon Guggenheim Memorial Foundation (HET), and the Brazilian Agencies FAPESP, CNPq and FAPEMIG is gratefully acknowledged.

References

[1] A. Juris, V. Balzani, F. Barigelletti, S. Campagna, P. Belser, A. Vonzelewsky, Coordination Chem. Rev. 84 (1988) 85.
[2] H. Yersin, D. Braun, Coordination Chem. Rev. 111 (1991) 39.
[3] V. Balzani, A. Juris, M. Venturi, S. Campagna, S. Serroni, Chem. Rev. 96 (1996) 759.
[4] M.K. Nazeeruddin, A. Kay, I. Rodicio, R. Humphrybaker, E. Muller, P. Liska, N. Vlachopoulos, M. Gratzel, J. Am. Chem. Soc. 115 (1993) 6382.
[5] K. Kalyanasundaram, M. Gratzel, Coordination Chem. Rev. 177 (1998) 347.
[6] A. Hagfeldt, M. Gratzel, Chem. Rev. 95 (1995) 49.
[7] S. Ferrere, B.A. Gregg, J. Am. Chem. Soc. 120 (1998) 843.
[8] F.M. Matsumoto, M.L.A. Temperini, H.E. Toma, Electrochimica Acta 39 (1994) 385.
[9] H.E. Toma, F.M. Matsumoto, C. Cipriano, J. Electroanal. Chem. 346 (1993) 261.
[10] C. Hidalgoluangdilok, A.B. Bocarsly, Inorganic Chem. 29 (1990) 2894.
[11] H.E. Toma, M.S. Takasugi, Polyhedron 1 (1982) 429.
[12] B. Kratochvil, E. Lorah, C. Garber, Anal. Chem. 41 (1969) 1793.
[13] ZINDO: A Comprehensive Semiempirical SCF/CI Package, Zerner, M.C. and co-workers, Quantum Theory Project, University of Florida Gainesville, USA.
[14] Cerius^2 version 3.8 environment, Molecular Simulation Inc. San Diego, USA, 1997.
[15] M.C. Zerner, G.H. Loew, R.F. Kirchner, U.T. Mueller-Westerhoff, J. Am. Chem. Soc. 102 (1980) 589.
[16] V.R.L. Constantino, H.E. Toma, L.F.C. de Oliveira, F.N. Rein, R.C. Rocha, D.D. Silva, J. Chem. Soc.-Dalton Trans. (1999) 1735.
[17] R. Pauncz, Spin Eigenfunctions, Plenum Press, NY, USA, 1979.
[18] N.L. Allinger, J. Am. Chem. Soc. 99 (1977) 8127.
[19] HyperChem Pro version 5.1, Hypercube Inc. Gainesville, USA, 1998.
[20] M.M. Karelson, M.C. Zerner, J. Phys. Chem. 96 (1992) 8991.
[21] J. Onuki, A.V. Ribas, M.H.G. Medeiros, K. Araki, H.E. Toma, L.H. Catalani, P. DiMascio, Photochem. Photobiol. 63 (1996) 272.
[22] V. Balzani, F. Scandola, Supramolecular Photochemistry, Ellis Horwood Chichester, UK, 1991, 44 pp.
[23] H.E. Toma, A.A. Batista, H.B. Gray, J. Am. Chem. Soc. 104 (1982) 7509.
[24] H.E. Toma, A.B.P. Lever, Inorganic Chem. 25 (1986) 176.